Solution Structure of the Chicken Cysteine-Rich Protein, CRP1, a Double-LIM Protein Implicated in Muscle Differentiation[†,‡]

Xiang Yao,[§] Gabriela C. Pérez-Alvarado,[§] Heather A. Louis,[∥] Pascal Pomiès,[∥] Catherine Hatt,[∥] Michael F. Summers,*[,§] and Mary C. Beckerle*[,∥]

Howard Hughes Medical Institute and Department of Chemistry and Biochemistry, University of Maryland Baltimore County, 1000 Hilltop Circle, Baltimore, Maryland 21250, and Department of Biology, University of Utah, Salt Lake City, Utah, 84112

Received August 21, 1998; Revised Manuscript Received January 22, 1999

ABSTRACT: The mechanism by which the contractile machinery of muscle is assembled and maintained is not well-understood. Members of the cysteine-rich protein (CRP) family have been implicated in these processes. Three vertebrate CRPs (CRP1−3) that exhibit developmentally regulated muscle-specific expression have been identified. All three proteins are associated with the actin cytoskeleton, and one has been shown to be required for striated muscle structure and function. The vertebrate CRPs identified to date display a similar molecular architecture; each protein is comprised of two tandemly arrayed LIM domains, protein-binding motifs found in a number of proteins with roles in cell differentiation. Each LIM domain coordinates two Zn(II) ions that are bound independently in CCHC (C═Cys, H═His) and CCCC modules. Here we describe the solution structure of chicken CRP1 determined by homonuclear and ^{1}H-^{15}N heteronuclear magnetic resonance spectroscopy. Comparison of the structures of the two LIM domains of CRP1 reveals a high degree of similarity in their tertiary folds. In addition, the two component LIM domains represent two completely independent folding units and exhibit no apparent interactions with each other. The structural independence and spatial separation of the two LIM domains of CRP1 are compatible with an adapter or linker role for the protein.

Muscle tissue is essential for the function of the locomotory, urogenital, circulatory, and respiratory systems in animals. However, the molecular machinery that controls the assembly and maintenance of the contractile elements within muscle cells is not well-understood. Recently, members of the cysteine-rich protein (CRP)[1] family have been shown to play critical roles in muscle differentiation and function. In vertebrates, three CRP family members, CRP1, CRP2, and CRP3, that display distinct patterns of muscle-specific expression have been identified. CRP1 is expressed in organs that are rich in both vascular and visceral smooth muscle (*1*, *2*). CRP2 appears to be most prominent in the vasculature (*1*, *3*), and CRP3, also referred to as the muscle LIM protein (MLP), is expressed in both cardiac and skeletal muscle (*1*, *4*). The importance of CRP3/MLP for striated muscle structure and function is now well-established (*4*, *5*). Elimination of CRP3/MLP function in the mouse by targeted gene disruption results in cardiac hypertrophy and disorganization of the myofibrillar arrays, events that compromise muscle function and lead to death of the organism (*5*). A role for CRP family members in muscle function does not appear to be confined to vertebrates. Two CRP family members have been identified in the fruitfly, *Drosophila melanogaster*, and both of these proteins are expressed exclusively in muscle derivatives and are upregulated during muscle differentiation and remodeling (*6*).

All CRP family members described to date exhibit similar molecular features. Each protein is comprised of an individual or a series of modules comprised of a LIM domain linked to a conserved glycine-rich region. The vertebrate CRPs each display two LIM-glycine modules and are very similar in overall sequence (*1*). Although the function of the glycine-rich region has not been established, LIM domains have been well-characterized.

LIM domains are comprised of approximately 60 residues, with the consensus sequence C-X_2-C-X_{16-23}-H-X_2-C-X_2-C-X_2-C-X_{16-21}-C-X_2-C/H/D (C = Cys, H = His, D = Asp, X = variable amino acid) (*7*). This cysteine-rich sequence was first identified in three homeodomain proteins, *Caenorhabditis elegans* Lin-11, rat Isl-1, and *C. elegans* Mec-3 (*8*, *9*), from which the term "LIM" is derived (*8*). Since the initial description of the LIM motif, a large number of proteins with diverse functions and subcellular distributions have been found to contain one to five copies of the LIM motif. Many LIM proteins have been shown to play central roles in cell differentiation pathways. For example, there are a number of LIM-homeodomain proteins that function as transcriptional regulators involved in specifying cell fates (*10*−*12*). Moreover, a group of proteins that are composed more or less exclusively of LIM domains also appear to contribute to developmental pathways. For example, the LIM-only protein LMO-2, or rhombotin-2, displays two LIM domains and is

[†]This work was supported by NIH Grant HL60591 (to M.C.B.).

[‡] Molecular coordinates have been deposited in Brookhaven Protein Data Bank (ID code 1b8t).

* To whom correspondence should be addressed. Phone: (410) 455-2527. Fax: (410) 455-1174. E-mail: summers@hhmi.umbc.edu.

[§] University of Maryland Baltimore County.

[∥] University of Utah.

[1] Abbreviations: CRP, cysteine-rich protein; 2D, two-dimensional; 3D, three-dimensional; HSQC, heteronuclear single quantum coherence spectroscopy; NOESY, nuclear Overhauser effect spectroscopy; TOCSY, total correlation spectroscopy; HOHAHA, homonuclear Hartmann−Hahn spectroscopy.

10.1021/bi982036y CCC: $18.00
Published on Web 04/14/1999

required as a transcriptional regulator in hematopoiesis (*13*). Likewise, as noted above, vertebrate CRP3/MLP is critical for differentiated muscle structure and function (*4, 5*).

Biophysical studies of LIM domains derived from a variety of proteins illustrated that each LIM domain specifically coordinates two zinc ions (*14*−*18*). In addition, the three-dimensional structures of several LIM domains, including two derived from different CRPs, have been solved (*19*−*22*). From these structural analyses, it is clear that all LIM domains examined to date consist of tightly packed CCHC and CCCC metal coordinating modules. Although the globular fold of the LIM domain is unique compared to the classical zinc finger proteins, the carboxy-terminal CCCC zinc-binding module of all known LIM domain structures is structurally similar to that observed for the DNA-interactive CCCC modules of the GATA-1 and Glucocorticoid receptor DNA binding (*23, 24*). Despite the structural similarity of LIM domains to nucleic acid-binding motifs, there is as yet no evidence for sequence-specific interactions between LIM domains and nucleic acids. In contrast, several LIM domains derived from different proteins have been shown to mediate specific associations with partner proteins (*7*, *25*−*31*).

In the case of the vertebrate CRPs, two protein partners that can bind all three CRP family members have been identified: zyxin (*1*, *18*) and α-actinin (*1*, *32*). Both zyxin and α-actinin are associated with the actin cytoskeletons of cells. α-Actinin is essential for muscle structure and function (*33*) and is localized at sites such as Z-disks of striated muscle and dense plaques of smooth muscle where actin filaments of the contractile machinery are anchored. Zyxin and α-actinin can themselves interact, and the two proteins are co-localized in fibroblasts and smooth muscle cells (*2, 34*). Domain mapping studies have revealed that both zyxin and α-actinin have docking sites within the N-terminal regions of the CRPs (*32, 35*). Thus, the N-terminal portions of the molecules serve as links to elements of the actin cytoskeleton. Although the C-terminal LIM-glycine module of each CRP is also predicted to have at least one protein partner, no proteins that interact with that region of the CRPs have yet been identified.

The functional conservation among CRPs that has been observed to date suggests that these proteins may be serving similar roles in different muscle derivatives where they are differentially expressed. Compelling genetic evidence for a key role of CRP3/MLP in cardiac muscle already exists (*36*), but the detailed role of the protein remains to be elucidated. Given the well-established involvement of LIM domains in protein−protein interactions, it has been proposed that the CRPs may serve as adapter proteins that link other protein components together (*4*, *7*, *18*, *32*). It has been suggested that CRP family members modulate muscle-specific gene expression (*4*, *37*) and/or perform a cytoarchitectural role in muscle (*5*, *32*).

Here we have determined the three-dimensional structure of chicken CRP1 by multidimensional nuclear magnetic resonance (NMR). This study provides the first structural description of a protein that displays multiple LIM domains. Comparison of the structures of the two individual LIM domains of CRP1 reveals a high degree of similarity in the tertiary folds of the two domains and has highlighted the importance of several residues in the overall packing and orientation of the zinc-binding modules. In addition, we show that the two component LIM domains of CRP1 represent two completely independent folding units and exhibit no interactions with each other. The structural independence and spatial separation of the two LIM domains of CRP1 suggest that they may function as independent units, compatible with an adapter or linker role for the protein. Thus our results have implications for understanding the central role of CRP1, and perhaps other CRP family members, in muscle function.

MATERIALS AND METHODS

Protein Expression, Purification, and Characterization. Plasmid-based expression constucts encoding full-length chicken CRP1 (aa 1−192), the N-terminal region (LIM1, aa 1−107), and the C-terminal region (LIM2, aa 108−192) were generated in pAED4 (LIM2) or pET5 (CRP1 and LIM1) as described previously (*14*, *15, 38*). Proteins were expressed in bacteria and purified to homogeneity. Briefly, the engineered expression vectors were introduced into *Escherichia coli* BL21(DE3) cells, and the cells were induced to produce the protein of interest by exposure to 0.4 mM isopropyl-*β*-D-thiogalactopyranoside (IPTG) (Sigma). Proteins were isolated from the bacterial cell lysates essentially as described previously (*1*, *14*, *16*, *32*). For CRP1 and LIM2, bacteria were lysed in 10 mM KCl, 10 mM potassium phosphate (pH 7.2), and 10 mM dithiothreitol, and soluble proteins were dialyzed versus column buffer (10 mM potassium phosphate (pH 7.2), 10 mM KCl, 0.01% 2-mercaptoethanol) prior to cation-exchange chromatography on CM-52 (Whatman); proteins were eluted from the column with a linear KCl (0−250 mM) gradient in column buffer. For LIM1, the soluble proteins and CM-52 column were pre-equilibrated in 5 mM potassium phosphate and 0.01% 2-mercaptoethanol. Column fractions containing purified proteins were pooled and lyophilized.

For production of ^{15}N-CRP1, bacteria were grown in M9 minimal medium containing 0.02 M ^{15}N-ammonium chloride (Isotec Inc., Miamisburg, OH) and supplemented as described previously (*20*). It was critical to grow the cells in three stages: initially a 1 mL culture was inoculated with bacterial cells harboring the CRP1 expression plasmid; on day 2, the starter culture was used to inoculate 100 mL of prewarmed medium and growth was continued overnight; in the final stage of growth, the stage 2 culture was used to inoculate 1 L of prewarmed medium containing 0.1 mM IPTG and incubated for 12 h prior to harvesting. Purification of ^{15}N-CRP1 was continued as described above.

Nuclear Magnetic Resonance Spectroscopy. Samples (4 mM LIM1; 2 mM CRP) for NMR were prepared in 90% H_2O/10% D_2O containing 50 mM KCl, 1 mM DTT, and 20 mM phosphate buffer (pH 7.2). NMR data were collected with a General Electric Omega PSG (599.71 MHz, ^{1}H) NMR spectrometer with the sample maintained at either 25 or 37.5 °C.

For Zn2-LIM1, 2D homonuclear Hartmann−Hahn (HOHAHA) spectra (75 ms MLEV-17 spin lock duration) were collected in the "clean" mode (*39*) using a continuous wave field to suppress water, followed by a Scuba train for partial recovery of presaturated H^α protons (*40*). A flip-back-homospoil train was added prior to the detection period to eliminate residual transverse water magnetization (*41*). 2D NOESY data were collected with a Dante-Scuba train and a

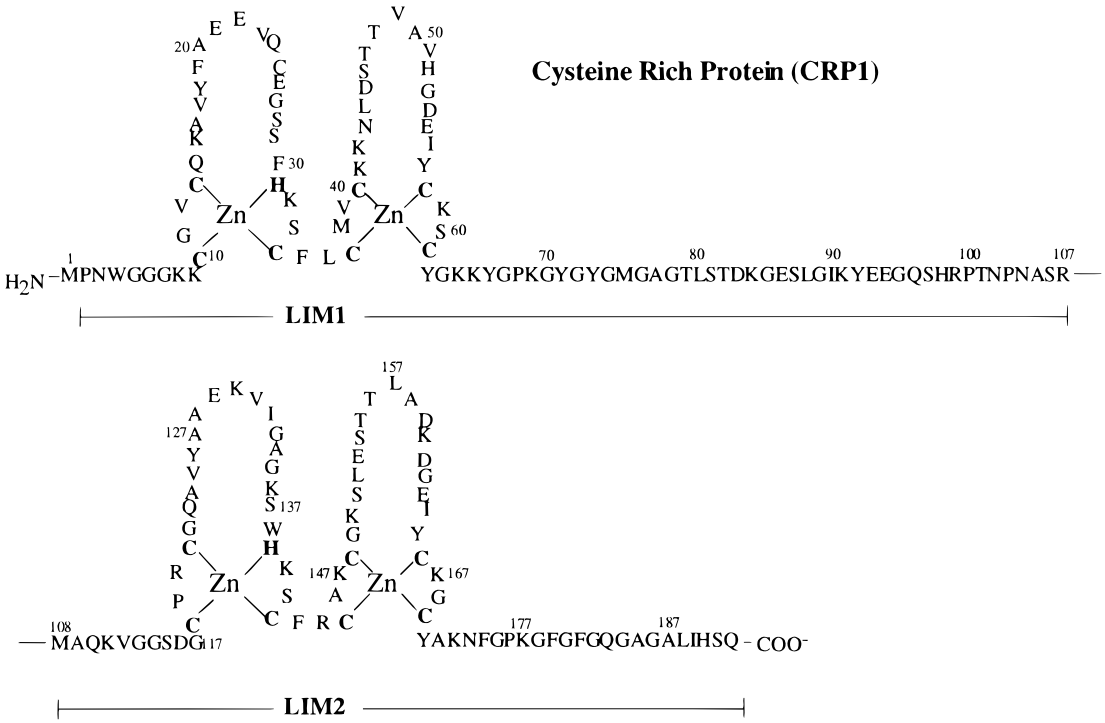

FIGURE 1: Diagram showing the amino acid sequence and metal-binding mode of the cysteine-rich protein (CRP1), comprising two tandemly arrayed LIM domains, LIM1 and LIM2.

homospoil-180° pulse-homospoil sequence centered in the 150 ms mixing period. 2QF-COSY spectra were obtained with a continuous wave field to suppress water, followed by a Scuba pulse train of 40 ms. The initial sampling delay for the data sets was set to half the t1 dwell period to eliminate baseline distortions in the F1 dimension (*42*, *43*). Also, the 2D-NOESY and cleanHOHAHA data sets were collected by alternating the real and imaginary data sampling in the t1 dimension to minimize t1 noise.

For CRP1, 2D ^{1}H homonuclear-correlated data were collected as described for LIM1, except that water suppression in the 2D NOESY and cleanHOHAHA experiments was achieved using a Shinnar-Leroux presaturation waveform (*44*), followed by a Scuba pulse train. 2D ^{1}H-^{15}N HSQC, 3D ^{1}H-^{15}N-NOESY-HSQC, and ^{1}H-^{15}N-cleanHOHAHA-HSQC spectra were acquired with a uniformly ^{15}N-labeled 2 mM CRP1 sample (90%H_2O/10%D_2O). The ^{1}H carrier was centered in the amide region (8.26 ppm) for all of the ^{1}H-^{15}N heteronuclear experiments in order to increase resolution in the F3 dimension (*45*), and water presaturation was performed using a 10 ms Shinnar-LeRoux phase-ramped waveform (*44*, *46*), followed by a 40 ms Scuba pulse train. The initial ^{15}N evolution period (F2) in all experiments was delayed by one-half of the dwell in order to remove baseline distortions (*47*, *48*). WALTZ-16 (*49*) modulation was used to decouple ^{15}N during acquisition with a field of 1−1.5 kHz. Other data collection parameters were as follows. ^{15}N-HSQC: 350 complex t1 data points, 400 μs t1 dwell. ^{15}N-NOESY-HSQC and ^{15}N-HOHAHA-HSQC: t1 (^{1}H), 32 scans per complex t1 increments, 128 complex points, 133 us t1 dwell; t2 (^{15}N), 32 complex points, 400 μs t2 dwell; t3 (^{1}H), 256 complex points, 270 μs dwell.

Data Processing and Analysis. NMR spectra were processed with the FELIX software (versions 2.05, 2.1, 2.3, and 95, Biosym Technologies, Inc.). The 2D cleanHOHAHA, COSY, and NOESY spectra collected on LIM1 were processed using a Kaiser window of size 2048 and an alpha parameter of 4 in t2, and using 80°-shifted squared sine bell filtering in t1 with zero filling to 2048 real data points in t1. Also, the NOESY and cleanHOHAHA data were processed using 40°-shifted squared sine bell filtering in t2, and 70°-shifted squared sine bell filtering in t1.

For data collected on CRP1, the 2D ^{1}H-^{15}N HSQC spectrum was processed with an 80°-shifted squared sine bell filter in t1, followed by zero filling to 1024 real data points. 3D ^{1}H-^{15}N-NOESY-HSQC and ^{1}H-^{15}N-cleanHOHAHA-HSQC spectra were processed using a Kaiser window apodization in t3. The data sizes were doubled by mirror-image linear prediction in t2, with apodization in t1 and t2 using 70°- and 80°-shifted squared sine bell and zero filled to 512 and 128 real points, respectively. All data analysis was performed with NMRVIEW software (*50*).

Structure Calculations. Structure calculations were carried out using the DYANA software package (*51*). Distance restraints of 1.8−2.7 Å, 1.8−3.3 Å, and 1.8−5.0 Å were employed for cross-peaks of strong, medium, and weak intensity, respectively, observed in the NOE spectra. An additional 0.5 Å was added for NOEs involving methyl protons (*52*), 0.8 Å was added for NOEs involving methylene protons, and 1.5 Å was added for NOEs involving degenerate valine methyls.

RESULTS

Sequence alignment of the CRP family members indicated that they share some common features which are not observed in other classes of LIM proteins (*53*). CRP proteins contain 192−194 residues and display two LIM domains, LIM1 (N-terminal) and LIM2 (C-terminal), which are separated by 56−59 residues (Figure 1). Sequence identity between family members is high. Each LIM domain contains

two zinc-binding modules, an N-terminal CCHC module, and a C-terminal CCCC module. Furthermore, a glycine-rich repeat in the adjacent sequence of the LIM motifs and a potential nuclear localization signal (KKYGPK) at residues 64−69 are found in all vertebrate CRPs. Direct sequence analysis revealed that the initiator methionine of CRP1 is removed post-translationally when the protein is isolated from chicken smooth muscle or when it is expressed in bacteria.

NMR Signal Assignments. Full-length chicken CRP1 (aa 1−192) and the N-terminal (LIM1, aa 1−107) and C-terminal (LIM2, aa 108−192) halves of the protein were expressed in bacteria and purified to homogeneity (Figure 2). The bacterially expressed proteins bound zinc with a ratio of two Zn(II) ions per LIM domain as determined by atomic absorbance spectroscopy.

NMR studies were carried out with nonlabeled recombinant Zn_2-LIM1 peptide and nonlabeled and ^{15}N-isotopically enriched recombinant Zn_4-CRP protein samples. Signal assignments were made by analysis of 2D homonuclear-correlated data, in combination with 2D and 3D ^{15}N-edited heteronuclear data (*54*, *55*). Careful comparison of the NMR data for LIM1, LIM2 (*19*), and CRP1 revealed that residues in both LIM1 and LIM2 peptides exhibit essentially identical chemical shifts and NOE cross-peak patterns with the corresponding residues in intact CRP1. Figure 3 shows good dispersion of ^{1}H-^{15}N HSQC spectrum collected for ^{15}N-labeled CRP1. Most of the ^{1}H-^{15}N correlations were observed for nonproline residues in CRP1. Signal degeneracies were largely resolved by ^{1}H-^{15}N-correlated NMR methods. An interesting observation, that residues in LIM1 give similar chemical shifts for equivalent residues in LIM2, was problematic in signal assignments for CRP. Nevertheless, with careful analysis of the combined 2D and 3D homonuclear and heteronuclear data, NH-NH, NH-H$^\alpha$, or NH-$^\delta$H (for proline residues) connectivities were observed for 109 of the 192 residues in CRP, enabling proton NMR signal assignments to be made via sequential assignment strategies (*54*, *55*). Residues Pro2-Gly7, Glu26-Gly27, Ser33, Ser46, Pro68-Asp116, and Pro176-Glu192 could not be assigned unambiguously due to internal motion or rapid chemical exchange with presaturated solvent protons.

Proton NMR signal assignments for most amino acid side chains were made by combination of 3D ^{1}H-^{15}N clean-HOHAHA-HSQC, 2D clean-HOHAHA, and 2QF-COSY data. In several cases, side-chain protons of residues with longer side chains could not be assigned unambiguously due to signal degeneracies and overlap. ^{1}H and ^{15}N chemical shift assignments are available in Supporting Information.

Secondary Structure Determination and Proton Chemical Shift Analysis. Elements of regular secondary structure were identified on the basis of cross-peak patterns and intensities observed in the 2D nuclear Overhauser effect (NOE) and the 3D ^{1}H-^{15}N-NOESY-HSQC spectra (*54*). The data obtained here for the C-terminal LIM domain of CRP1 (LIM2) is essentially identical to that reported previously for the recombinant C-terminal fragment (residues 109−192) (*19*), and will not be discussed here. The LIM1 domain of CRP1 exhibited strong sequential NH-H$^\alpha$ NOE connectivities for residues Lys9-Gly11, Lys15-Tyr18, Glu22-Cys25, Ser28-Lys32, Phe35-Met38, Lys42-Asp45, Val49-His52, and Glu55-Lys59 segments, indicating that these segments exist in an

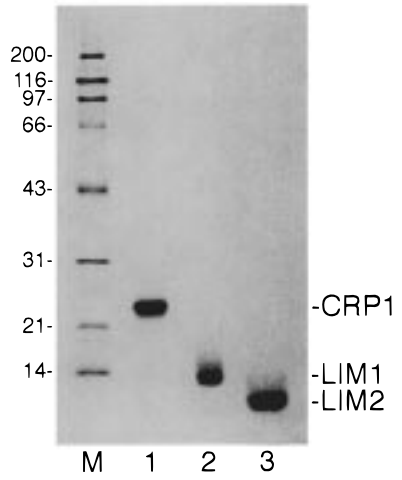

FIGURE 2: Expression and purification of CRP1 (lane 1), LIM1 (lane 2), and LIM2 (lane 3). A Coomassie blue-stained sodium dodecyl sulfate−polyacrylamide gel showing purified CRP1 and the LIM1 (aa 1−107) and LIM2 (aa 108−192) subregions. The three polypeptides were expressed in bacteria and purified to apparent homogeneity by ion-exchange chromatography.

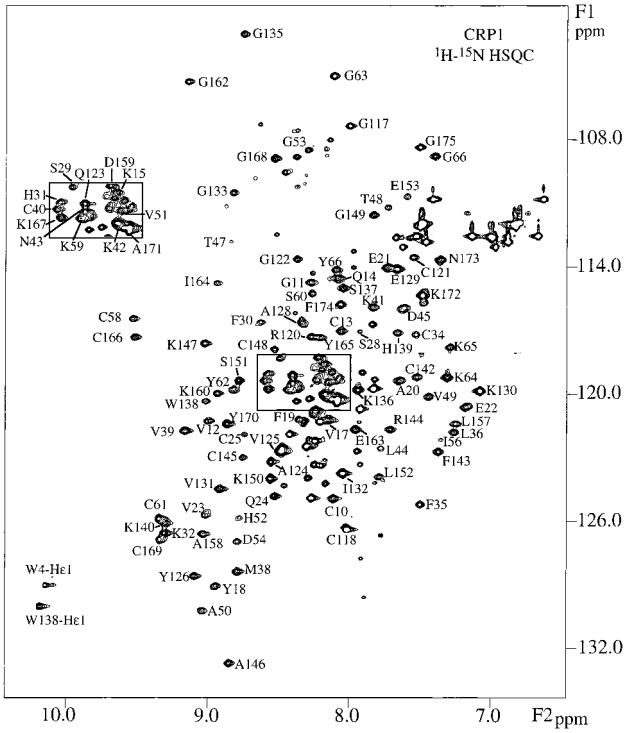

FIGURE 3: Portion of the 2D ^{1}H-^{15}N-HSQC spectra of ^{15}N-CRP1 (pH 7.2, T = 25.0 °C, 90%H_2O/10%D_2O). The spectrum shows ^{1}H-^{15}N correlations for 106 of the nonproline residues.

extended conformation (β1 through β8, respectively). Figure 4 illustrates the sequential NOE connectivities defining β5 and β6 containing residues Phe35-Asp45. Strong interstrand H$^\alpha$-H$^\alpha$ NOEs characteristic of antiparallel β-sheet structure further define the eight β strands into four sequential antiparallel β sheets (sheets I−IV), schematically shown in Figure 5. NOE cross-peaks characteristic of an α-helix were observed for residues Lys59-Gly67. For example, strong- to medium-intensity sequential NH-NH and weak NH(i)-H$^\alpha$(i + (2−4)) NOEs were observed for most of the residues in this stretch. Characteristic medium-intensity H$^\alpha$(i)-H$^\beta$(i + 3) NOEs were only observed for Cys61-H$^\alpha$ and β protons of Lys64 due to signal overlap.

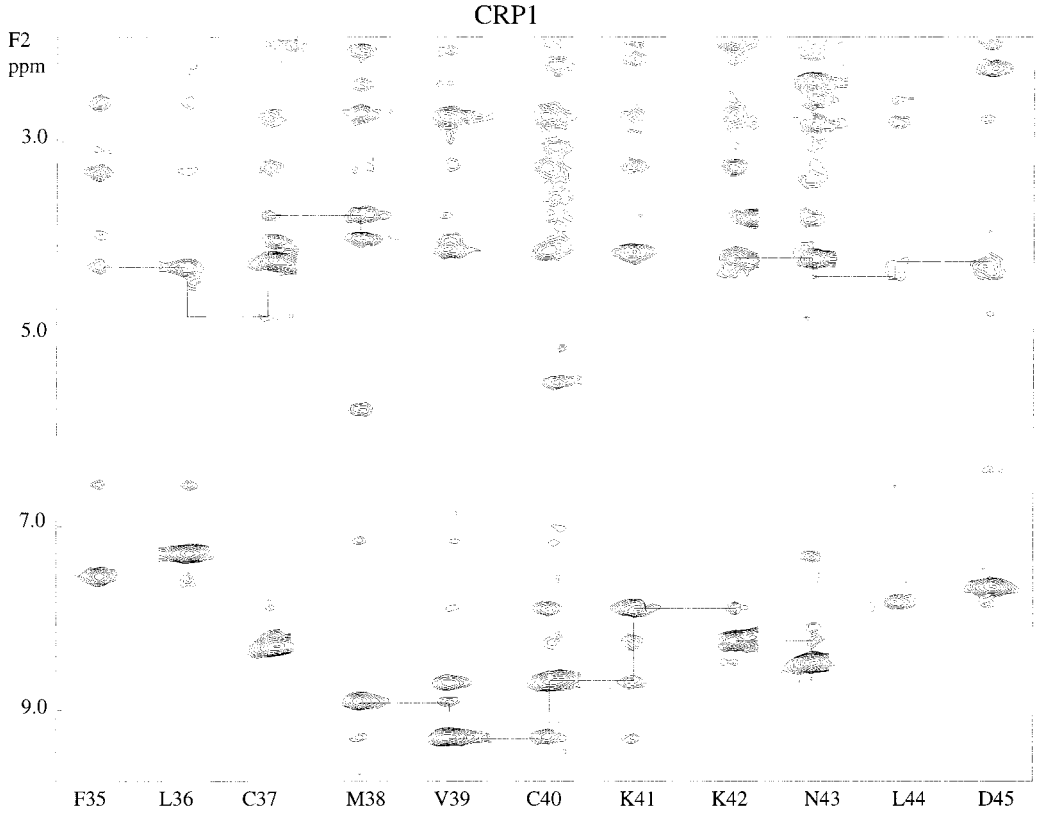

FIGURE 4: Strips from the 3D ^{1}H-^{15}N-NOESY-HSQC spectrum of ^{15}N-CRP1 (pH 7.2, $T = 25.0$ °C, $t_m = 150$ ms, 90%H_2O/10%D_2O) taken at the ^{15}N chemical shifts of residues Phe35 to Asp45, corresponding to β5 and β6, characterized by strong sequential H$^{\alpha}$-NH connectivities denoted by solid lines (top). Strong sequential NH-NH connectivities (bottom) for residues Met38-Lys42 are consistent with a Rd-Knuckle.

Residues Cys10-Lys15 and Cys37-Lys42 display NOEs characteristic of metal-coordinating Cys(i)-X(i + 1)-X(i + 2)-Cys(i + 3)-Gly-X(i + 5) "rubredoxin knuckles" (*19*, *56*, *57*). Thus, strong H$^{\alpha}$-HN NOEs were observed for Cys10-Gly11 and Cys37-Met38 proton pairs. Strong sequential NH-NH NOEs for residues Gly11-Lys15 and Met38-Lys42 (Figure 4) are also consistent with a Rd-knuckle.

Strong- and medium-range sequential NH-NH NOEs for Ala20-Glu22 and medium-intensity Ala20-H$^{\alpha}$-Glu21-NH NOE indicate that β sheets I and II are linked by a type I′ turn. NOEs characteristic for a type II turn were observed for residues in sheet IV, including strong- to medium-intensity NOEs for Gly53-H$^{\alpha}$-Asp54-NH and Asp54-NH-Glu55-NH proton pairs. NOE patterns for residues Lys32 to Cys34 suggest that this segment exists as a tight turn. However, the absence of assignments for residue Ser33 precluded unambiguous identification of the specific definition of the β turn type. In addition, secondary structure for residues connecting β3 with β4 and β6 with β7 could not be identified due to lack of assignments for Glu26-Gly27 and Ser46. The NOE connectivities for backbone protons and selected side-chain protons and corresponding secondary structural elements are summarized in Figure 6.

It has previously been shown that NMR chemical shifts for backbone H$^{\alpha}$ atoms correlate with secondary structure (*58*−*60*). Therefore, chemical shift values of the H$^{\alpha}$ resonances of CRP were compared with the random coil values. With a few exceptions, the resulting secondary shifts generally agree with the secondary structure derived from the NOE data (Figure 6). Specifically, residues Val23 to Gln24, Ser28 to His31, Val49 to His52, and Glu55 to Cys58 exhibit positive secondary shifts consistent with an extended conformation, and residues Lys59 to Tyr66 exhibit negative secondary shifts consistent with a helical structure.

Structure Determination. A total of 949 experimental distance restraints derived from 2D and 3D NOE data were employed for structure calculations of CRP1, including 60 intraresidue, 234 sequential, 198 medium-range (2−5 residues), 241 long-range interproton distance restraints, and 216 NH−O and N−O hydrogen bond restraints (Table 1). Hydrogen bonding restraints were determined from analysis of the NOE-derived secondary structure. To enforce Zn−S and Zn−N bond distances of 2.3 and 2.0 Å, respectively, and to ensure proper hybridization of the His-N$^{\delta}$ and Cys-S$^{\gamma}$ atoms, we included 68 distance restraints in the structural calculation. Protons that exhibit NOE cross-peaks to a specific prochiral proton often give a signal to the neighboring prochiral proton, and in the present studies, restraints were not included for the weaker of two such cross-peaks. Restraints for moderate or weak intraresidue cross-peaks, which do not serve a useful function in the structure calculations, were also not included. No intraresidue restraints were imposed for side-chain protons with undefined stereochemistry. Thus, many cross-peaks observed in the NOE spectra were not used as distance restraints. On average, a total of 16.4 distance restraints per assigned residue were used for structure calculations. The total number of NOE-derived interproton distance restraints as a function of residue number is shown in Figure 7.

A family of 46 refined conformers was generated, with individual distance violations of 0.17 Å or less and penalty values (= squared sum of all distance violations) of 0.17−0.21 Å^2 (Table 1). Of these, 9 structures were generated without hydrogen bond restraints. Models generated with and

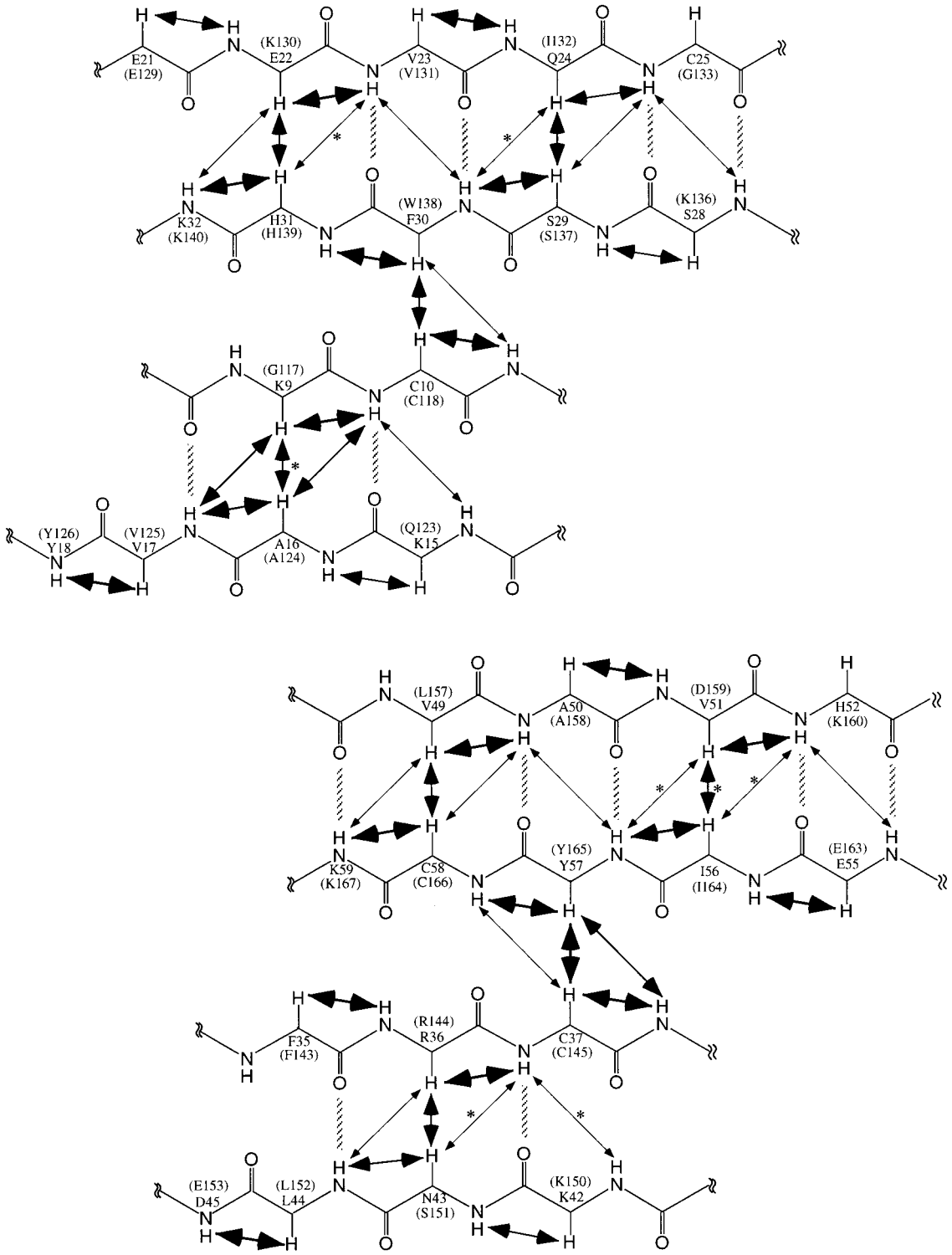

FIGURE 5: Schematic representation of the characteristic NOE connectivities (arrows) that define the four sequential antiparallel β-sheets of each LIM domain in CRP1. The thickness of the arrows is proportional to the intensity of the cross-peaks. Hydrogen bonds deduced from the NOE data and modeling studies are denoted as lines. Stars indicate NOE connectivities for which insufficient evidence is available due to signal degeneracy or overlap. These were not included in structure calculations.

without hydrogen bond restraints exhibit the same three-dimensional structures. The relative orientation of LIM1 and LIM2 in the context of CRP1 could not be defined uniquely due to the absence of signal assignments for the linker region between the two LIM domains. Therefore, structural convergence was evaluated for the individual domains. Best-fit superposition of restrained residues in LIM1, including residues Cys10-Val17, Glu22-Cys25, Ser28-Leu44, and Thr48-Gly63 of all 37 models, afforded an average pairwise rms deviation of 0.84 (±0.30) Å (Figure 8). Best-fit superpositions of restrained residues in LIM2, including residues Asp116-Val125, Glu129-Glu153, and Leu157-Ala171 of all 37 models, afforded an average pairwise rms deviation of 0.85 (±0.37) Å (Figure 9). As observed previously for the C-terminal fragment of CRP1 (*19*), superposition of the individual N- and C-terminal zinc-

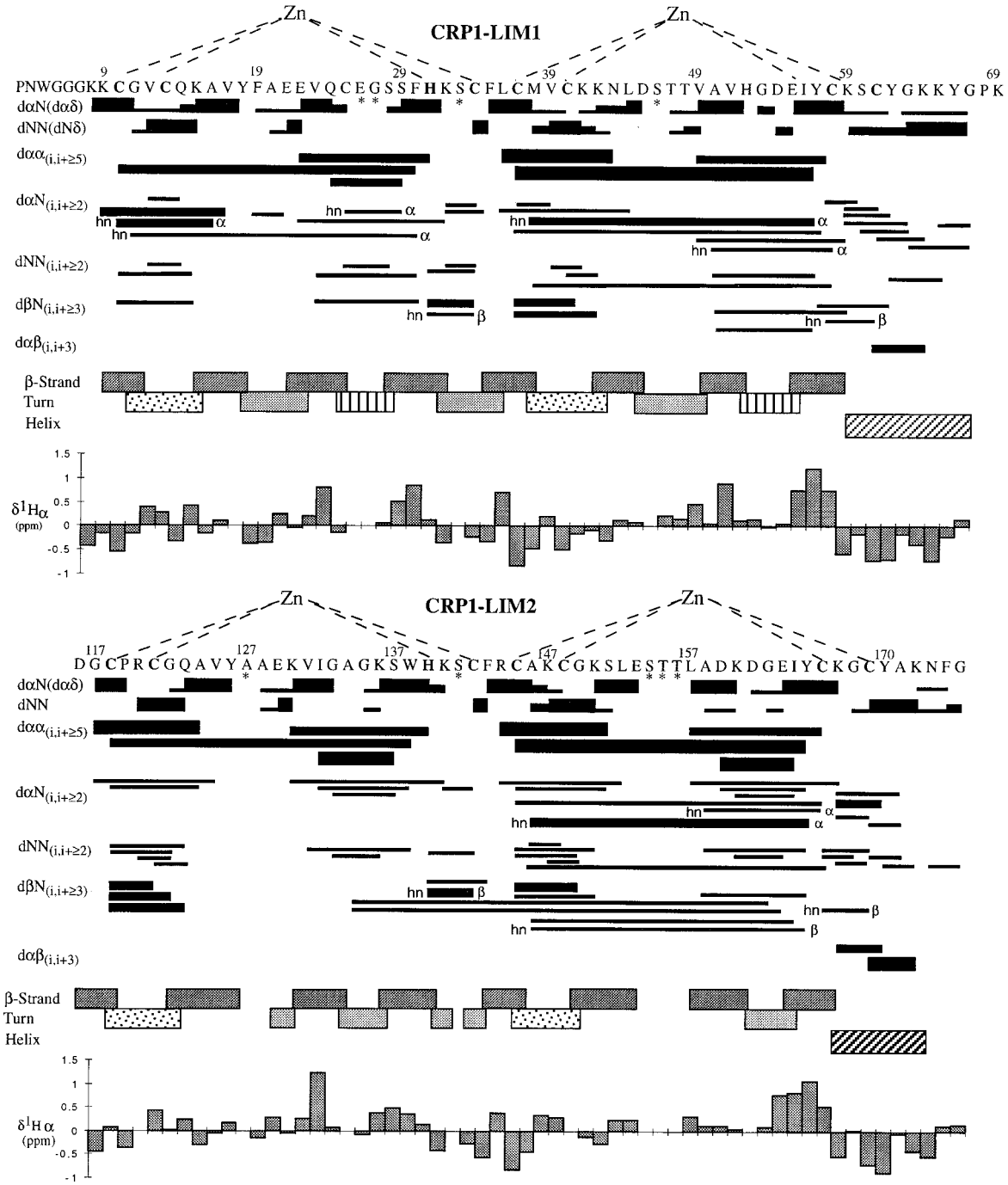

FIGURE 6: Summary of H^{α}-NH, NH-NH, and H^{α}- H^{α} NOE connectivities identified from 2D NOESY spectra and 3D ^{1}H-^{15}N-NOESY-HSQC spectra of LIM1 and LIM2 peptides and CRP1. The thickness of the horizontal bars denotes the relative intensities of the NOE cross-peaks. The secondary structural elements for each LIM domain are also shown. The α-proton secondary chemical shifts are shown at the bottom of each figure. Groupings of downfield-shifted protons (>0) correspond to *β*-strand type structure; upfield-shifted groups (<0) correspond to helical structure.

binding modules of LIM1 and LIM2 results in lower rmsd values (Table 1), suggesting that flexibility may exist at the interfaces of the zinc-binding modules of both LIM domains.

Description of the Three-Dimensional Structure of CRP1. The LIM1 and LIM2 domains of intact CRP1 exhibit tertiary structures that are essentially identical to the structure determined for the isolated N-terminal and C-terminal fragments. The best convergence was obtained for intact CRP1 because the protein was N^{15}-labeled, enabling the collection and analysis of 3D NMR data, the resolution of signals that overlapped in the 2D data, and the identification of additional NOE cross-peaks.

As we observed previously for the LIM2 region of CRP1 (*19*), LIM1 consists of N-terminal CCHC (Cys10-Cys34) and C-terminal CCCC modules (Cys37-Cys61) packed together via a hydrophobic interface. The structures of the two zinc-binding modules of LIM1 are similar to those of LIM2 (Figure 10). Within the CCHC module of LIM1, residues Lys9 to Val17 form an antiparallel *β*-sheet with a Rd-knuckle, followed by a turn structure (Tyr18-Glu22) that leads to a second *β*-sheet (Val23-His31), which is almost perpendicular relative to the first *β*-sheet. The CCHC module is linked with the CCCC module by a short turn formed by residues His31 to Cys34. Residues Phe35-Leu44 comprise

Table 1. Distance Geometry Restraints and Structural Statistics[a]

Distance Restraints	
intraresidue	60
sequential	234
medium range ($|i-j|$2−5 residues)	198
long range ($\|i-j\|$ >5 residues)	241
hygrogen bonds	216
metal−ligand	68
total NMR-derived restraints	949
mean restraints per residue	16.4
Distance Violations[b]	
mean total penalty	0.20 ± 0.01 Å^2
maximum total penalty	0.21 Å^2
minimum total penalty	0.17 Å^2
max individual violation	<0.17 Å

Pairwise Rms Deviations (Å)[b]

	H-bonds[c]		all structures[d]	
	backbone atoms[e]	all atoms[f]	backbone atoms[e]	all atoms[f]
residues 10−34[g]	0.46 ± 0.13	1.16 ± 0.21	0.54 ± 0.16	1.21 ± 0.21
residues 35−63[h]	0.51 ± 0.16	1.16 ± 0.22	0.66 ± 0.27	1.30 ± 0.28
residues 10−63[i]	0.84 ± 0.30	1.41 ± 0.29	0.95 ± 0.32	1.51 ± 0.31
residues 116−142[j]	0.36 ± 0.11	1.09 ± 0.19	0.69 ± 0.50	1.28 ± 0.36
residues 143−171[k]	0.59 ± 0.23	1.31 ± 0.26	0.56 ± 0.23	1.22 ± 0.25
residues 116−171[l]	0.85 ± 0.37	1.44 ± 0.33	0.97 ± 0.42	1.48 ± 0.34

[a] Penalty (equal to the squared sum of the distance violations) and rmsd values are in units of Å^2 and Å, respectively; distance violations are in units of Å. Values are reported as a mean ± standard deviation. [b] Results for 46 structures generated by the program DYANA (Dynamics Algorithm for NMR Applications), including 37 generated with H-bond restraints and 9 without H-bond restraints. [c] Results for 37 structures generated by the program DYANA (Dynamics Algorithm for NMR Applications), with H-bond restraints. [d] Results for all 46 structures, including 37 generated with H-bond restraints and 9 without H-bond restraints. [e] Average of pairwise rms deviations relative to each of the stuctures calculated from the superposition of backbone C, Ca, and N atoms for the given range of residues. [f] Average of pairwise rms deviations relative to each of the stuctures calculated from the superposition of all atoms for the given range of residues. [g] Residues comprising the N-terminal CCHC module of LIM1. Rms deviations for backbone atoms were calculated for residues Cys10-Val17, Glu22-Cys25, and Ser28-Cys34. [h] Residues comprising the C-terminal CCCC module of LIM1. Rms deviations for backbone atoms were calculated for residues Phe35 -Leu44 and Thr48-Gly63. [i] The entire folded LIM1. Rms deviations for backbone atoms were caculated for residues Cys10-Val17, Glu22-Cys25, Ser28-Leu44, and Thr48-Gly63. [j] Residues comprising the N-terminal CCHC module of LIM2. Rms deviations for backbone atoms were calculated for residues Asp116-Val125, Lys130-Ile132, and Gly135-Cys142. [k] Residues comprising the C-terminal CCCC module of LIM2. Rms deviations for backbone atoms were caculated for residues Phe143-Leu152, Leu157-Lys160, and Glu163-Ala171. [l] The entire folded LIM2. Rms deviations for backbone atoms were caculated for residues Asp116-Val125, Lys130-Ile132, Gly135-Leu152, Leu157-Lys160, and Glu163-Ala171.

the third antiparallel β-sheet that also contains a Rd-knuckle, and residues Val49-Lys59 form a fourth antiparallel β-sheet, followed by an α-helix formed by Lys59-Gly67.

Within the CCHC module of LIM1, the backbone amide protons of Val12, Cys13, and His31 form hydrogen bonds to the Cys10-S$^\gamma$ sulfur, and the backbone amide protons of Lys15 forms a hydrogen bond with the S$^\gamma$ atom of Cys13. His31 coordinates to zinc through the Nδ1 nitrogen, and the presence of strong NOEs between the His31-H$^{\delta 2}$ and the Glu21-H$^\beta$, H$^\gamma$ protons indicates that the Glu21 side chain carboxyl group is hydrogen-bonded to the His31-NH$^{\epsilon 2}$ proton. The backbone amide protons of residues Val39, Cys40, and Cys58 of the CCCC module form NH−S hydrogen bonds to the S$^\gamma$ atom of Cys37, and the backbone amides of Lys42 and Cys61 form hydrogen bonds to the S$^\gamma$ atoms of Cys40 and Cys59, respectively. Identical H-bonding patterns can be deduced from NOE data of CRP1-LIM2, and direct evidence for the existence of these NH−S hydrogen bonds was previously obtained for the recombinant LIM2 peptide (*19*). These results are consistent with the recent work on both the wild type and a point mutant of the C-terminal LIM domain of Quail CRP2 (*61*). Additional H-bonding networks surrounding the CCHC and CCCC modules of the LIM domain proposed therein could not be unambiguously confirmed in CRP1 due to signal overlap and degeneracies.

While the overall folds of the two LIM domains are very similar, there is one noticeable difference occurring at the interface of the N- and C-terminal zinc-binding modules of the individual LIM domains. In LIM2, the two modules pack more tightly against each other than their counterparts in LIM1, mainly due to multiple hydrophobic interactions between residues in the second and the fourth β-sheets of LIM2, whereas a wider cleft is observed between β-sheet II and IV of LIM1 due to lack of such interactions. As occurs in LIM2, the CCHC and CCCC modules of LIM1 pack together via a hydrophobic interface formed by side chains of residues Val12, Val23, Phe30, Phe35, Leu44, Val49, Val51, and Ile56. Of these residues, Phe30, Phe35, Leu44, and Val49 are absolutely conserved throughout the CRP family. Interestingly, positions corresponding to Phe30, Phe35, and Leu44 are conservatively substituted in all of the LIM sequences characterized to date, suggesting that these hydrophobic residues are important determinants for the overall folding of the LIM domain. Other residues that contribute to the hydrophobic core of LIM1 including Val12, Phe30, Val49, and Val51 are not conserved; in LIM2, these residues are replaced by Arg120, Trp138, Leu157, and Asp159 at the corresponding positions within the LIM domain. These substitutions may contribute to the structural differences observed between LIM1 and LIM2. In addition, Ala134, which is located within β-sheet II and forms several hydrophobic interactions with residues in β-sheet IV in LIM2, is substituted by the acidic residue Glu26 at the corresponding position of LIM1. This substitution appears to be a major factor that contributes to the differences in the relative orientations of the CCHC and CCCC modules in the two LIM domains of CRP1.

DISCUSSION

Here we have determined the structure of a native protein that displays two LIM domains. Members of the vertebrate CRP family display muscle-specific expression and are postulated to play central roles in the organization and function of these contractile tissues (*1*, *4*, *5*). The most striking demonstration of the requirement for a CRP family member for muscle development comes from studies on CRP3/MLP in the mouse (*5*, *36*). When both copies of the gene encoding CRP3 are disrupted by homologous recombination, striated muscle appears to differentiate normally but it seems to lack the mechanical stability to withstand the forces generated during vigorous post-natal muscle contraction. In the case of cardiac muscle, where the phenotype is particularly severe, hypertrophy ensues and muscle function is further compromised leading to death. Although the importance of at least this one CRP family

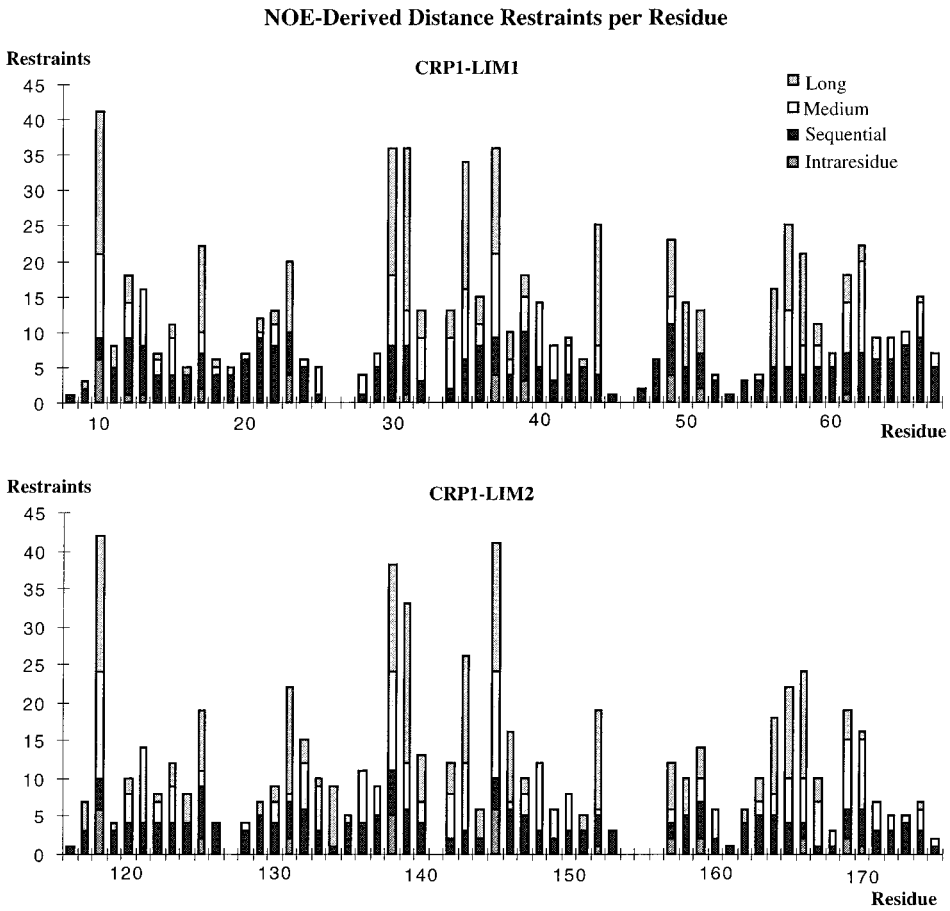

FIGURE 7: Plot showing the number of intraresidue, sequential (i to $i + 1$), medium-range (i to $i + 2-5$), and long-range (i to $i > 5$) NOE-derived interproton distance restraints per residue employed for structural calculations of CRP1.

member for muscle function is quite clear, little is understood about the molecular nature of its role within the muscle cell. Nevertheless, the high degree of sequence similarity among the three vertebrate CRPs suggests that they may play similar roles in different muscle subtypes. Because CRP family members are comprised more or less exclusively of LIM domains, we sought to define the three-dimensional solution structure of one family member, CRP1, in an effort to gain insight into how it might operate in vivo.

Analysis of the structure of CRP1 revealed that the two component LIM domains exist as independent structural motifs within the native protein. The tertiary folds of the LIM domains are not influenced by each other as evidenced by the fact that their conformations are the same whether they are expressed as isolated modules or as part of the full-length protein. No interactions between the individual LIM domains were observed in solution. One hypothesis for the function of CRP family members is that they serve to cross-link key elements of the muscle contractile machinery, thus stabilizing them against the forces that are generated during muscle contraction (*32*). The solution structure of CRP1 is compatible with this model. Individual LIM domains have been shown to function to dock specific protein partners (*7*, *28*). The observations that the two LIM domains in CRP1 fold completely independently and that they are connected by a flexible linker region suggest that the two tandemly arrayed LIM domains may be able to interact simultaneously with distinct binding partners that are distantly spaced, thus enabling the full-length protein to act as a linker or adapter molecule. It is also conceivable that, once their biological partners are present, the two LIM domains might be brought closer together to allow for the assembly of a protein complex, and CRP1 may then assume a more compact structure.

Biochemical studies have led to the identification of two binding partners for vertebrate CRP family members. The first CRP-binding partner to be recognized was zyxin, a protein that is co-localized with CRPs in association with actin filaments and at sites of actin−membrane linkage; one of zyxin's functions may be to regulate actin assembly and organization (*62*). CRP family members also interact with a well-characterized actin cross-linking protein called α-actinin (*1*, *32*). Interestingly, domain mapping studies have revealed that the LIM1 region of CRP1 is sufficient to support its ability to associate with α-actinin, and this region also harbors information that targets it to elements of the actin cytoskeleton in vivo (*32*). Zyxin's binding site on CRP1 is not as discrete but nevertheless appears focused primarily on the N-terminal part of the protein (*38*). Thus, one can envision the N-terminal domain of CRP1 as an element that allows the protein to associate with the actin cytoskeleton (Figure 11), a primary constituent of the contractile machinery of a muscle cell. On the basis of the structural studies described here for purified CRP1 in solution, one can imagine that the C-terminal LIM domain of CRP1 might be available for docking an additional partner. If this were the case, CRP1 could then serve to cross-link two elements within the muscle, the actin cytoskeleton and some other molecular

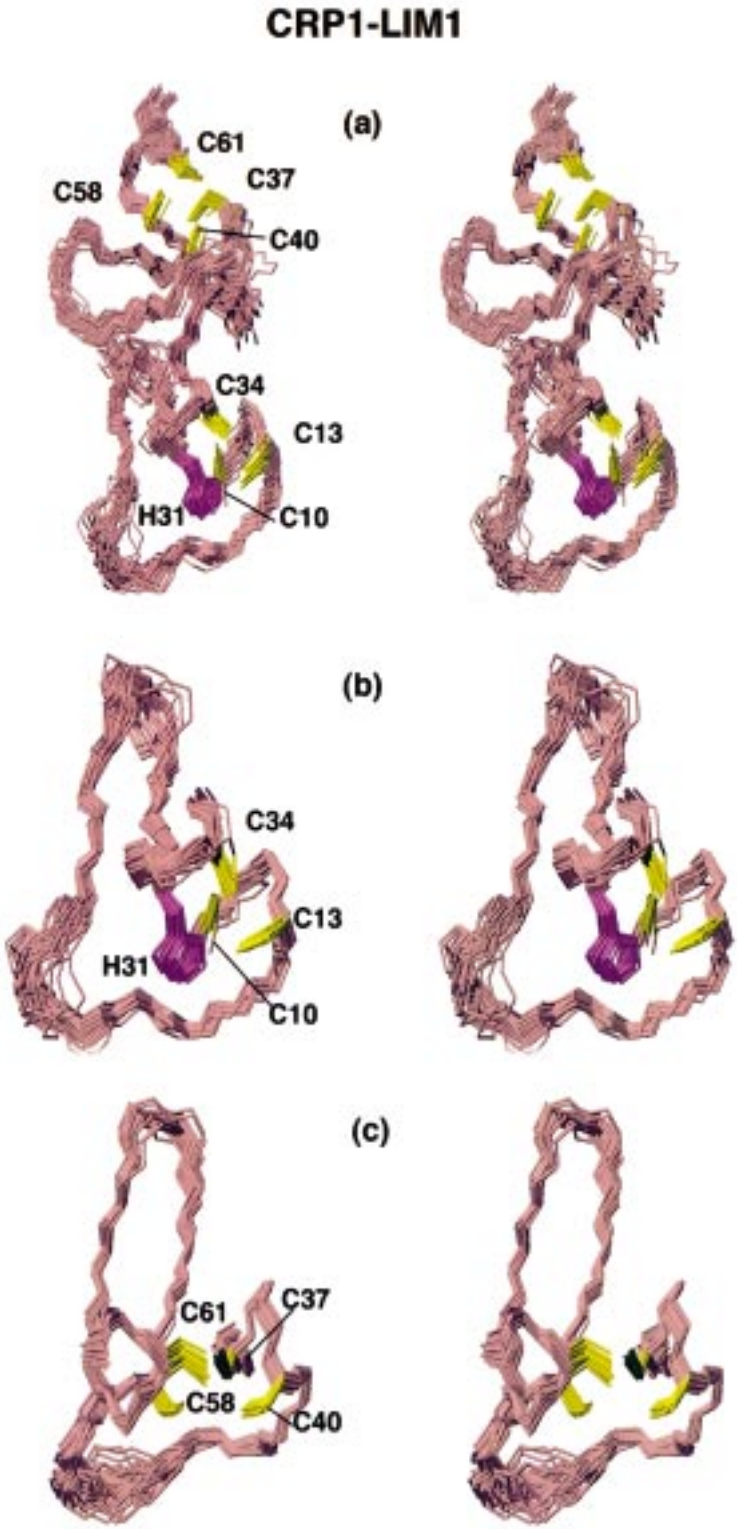

FIGURE 8: Stereoviews of the best-fit superpositions of the backbone heavy atoms C, C^{α}, and N, and (a) Cys10-Val17, Glu22-Cys25, Ser28-Leu44, and Thr48-Gly63 of the entire folded LIM1 domain; (b) residues Cys10-Val17, Glu22-Cys25, and Ser28-Cys34 of the N-terminal CCHC module; and (c) Phe35-Leu44 and Thr48-Gly63 of the C-terminal CCCC module of LIM1 domain for 37 refined CRP1 models generated with hydrogen-bond restraints. Side-chain heavy atoms of metal ligands are shown with cysteine residues in yellow and histidine residues in red. Figures were generated with the MOLMOL software package.

feature. On the basis of the loss of function phenotype for CRP3/MLP in striated muscle, one would predict that the CRP-dependent linkage of these elements would stabilize the muscle cytoarchitecture in a fashion that is essential for the ongoing contractile function of the muscle cells. Identification of partners for the LIM2 region of the vertebrate CRPs is likely to enhance significantly our understanding of the physiological role of these proteins in muscle.

In addition to the now well-established role of LIM domains in specific protein−protein interactions, LIM domains have also been postulated to interact with nucleic acids. The CCCC modules of all of the LIM domains characterized

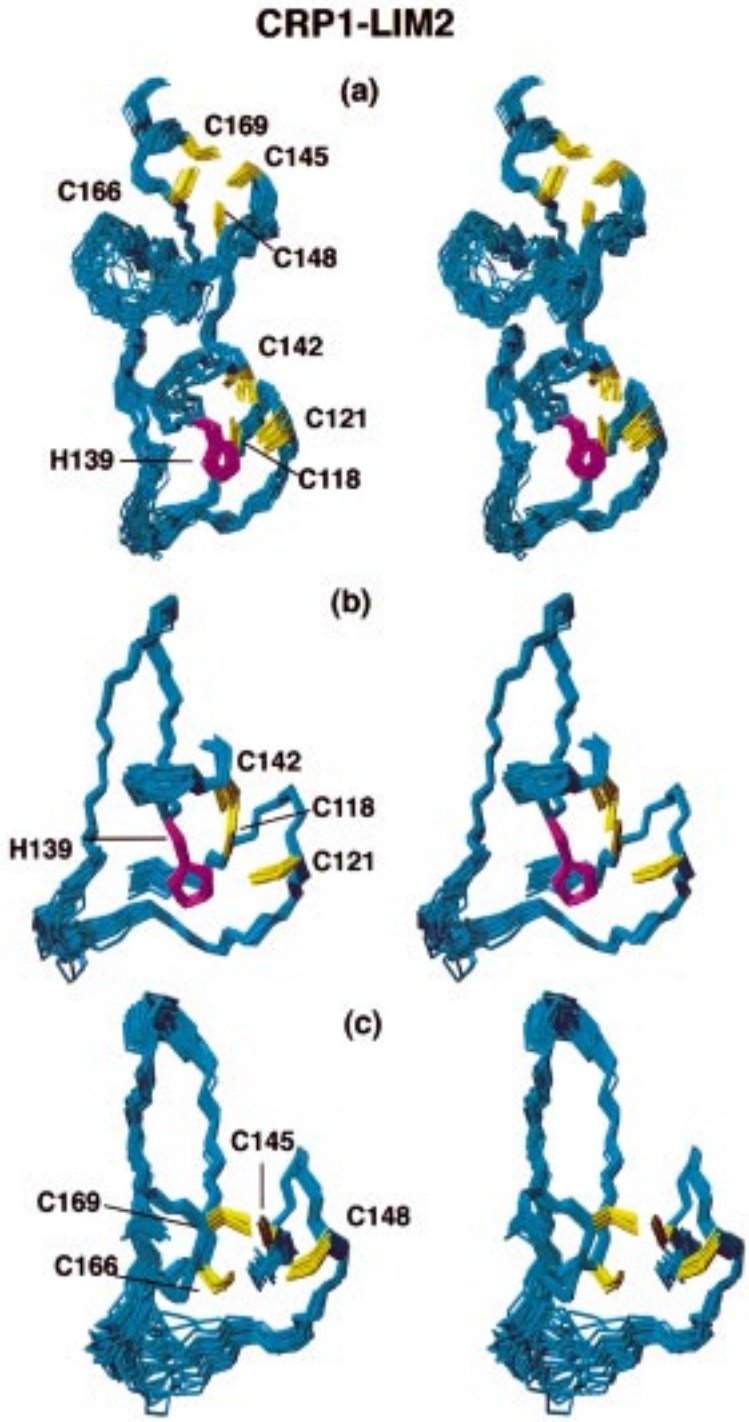

FIGURE 9: Stereoviews of the best-fit superpositions of the backbone heavy atoms C, C^{α}, and N, and (a) residues Asp116-Val125, Lys130-Ile132, Gly135-Leu152, Leu157-Lys160, and Glu163-Ala171 of the entire folded LIM2 domain; (b) residues Asp116-Val125, Lys130-Ile132, and Gly135-Cys142 of the N-terminal CCHC module; and (c) Phe143-Leu152 and Leu157-Lys160 of the C-terminal CCCC module of LIM2 domain for 37 refined CRP1 models generated with hydrogen-bond restraints. Side-chain heavy atoms of metal ligands are shown with cysteine residues in yellow and histidine residues in red. Figures were generated with the MOLMOL software package.

to date, including both LIM domains of CRP1, adopt tertiary folds that are very similar to the DNA-binding modules of the GATA-1 and GR DBDs (*23*, *24*). These structural similarities suggest that the conformation of the LIM domain may be compatible with nucleic acid binding. The functional significance of these structural relationships is not yet clear. To date, only one example of nucleic acid binding by a LIM domain has been described (*63*) and evidence of sequence-specific nucleic acid binding by a LIM domain has not been reported. However, it is of potential interest that the CCCC metal-binding module may play a less significant role in defining the protein-binding specificity of the LIM domain than does the N-terminal CCHC module (*35*). At present it is not known whether the physiological roles of any LIM domains might rely on nucleic acid-binding capacity.

The structural results reported here also shed some light on the question of whether the LIM domains of CRP family members homo-oligomerize. On the basis of positive results in a two-hybrid screen in which CRP1 was used both as bait and prey, it was suggested that the protein may be able to

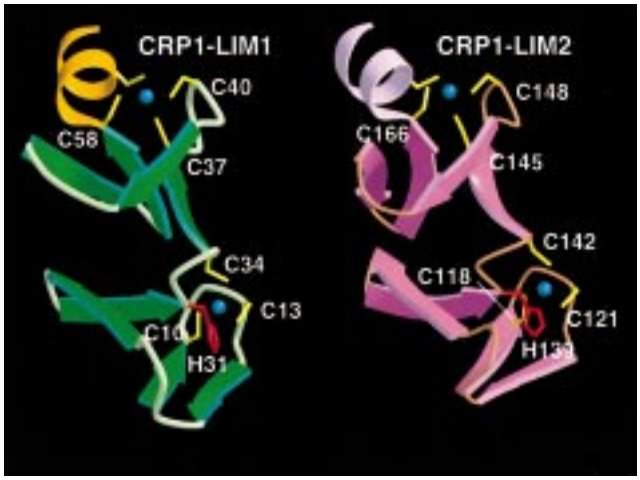

FIGURE 10: Ribbon drawing of each LIM domain of CRP1 structure with the lowest distance restraint violations. Metal ligands are represented with cysteine residues in yellow and histidine residues in red. Zinc atoms are shown by blue spheres. Figures were generated and rendered with the MOLSCRIPT (*64*) and Raster3-D (*65*) software packages, respectively.

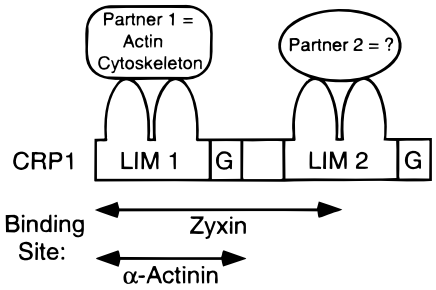

FIGURE 11: A model for CRP1 function. On the basis of biochemical studies as well as our structural studies that show the spatial independence of the N-terminal and C-terminal LIM domains of CRP1, we suggest that CRP1 may be able to dock constituents of the actin cytoskeleton via its N-terminal region and some as yet unidentified component via its C-terminal region. Such simultaneous association of CRP1 with multiple protein partners could recruit regulatory molecules to the actin framework, or it could serve to link the actin cytoskeleton to some other structural element in the muscle cell.

self-associate via LIM-LIM interactions (*25*). However, in apparent contrast with those findings, hydrodynamic studies of purified CRP1 suggested that the native protein is monomeric at physiological ionic strength (*2*). Likewise, we have detected no evidence for dimerization of CRP1 by NMR under conditions where protein concentrations are very high. Because the two hybrid interactions were observed in the context of an intact mammalian cell, it is possible that cellular proteins may mediate the association between the LIM domains of CRP1 that was detected by that method.

Although LIM domain structures appear to be very similar overall, our studies reveal a small but significant difference between the relative orientations of the CCHC and CCCC modules of the LIM domains of CRP1. More extensive hydrophobic interactions between the two modules of LIM2 result in a more compact structure than LIM1. Comparison of the tertiary structures of the two LIM domains of CRP1 with the single LIM domain protein CRIP (*20*) indicates that, while the corresponding zinc-binding modules in these LIM domains are structurally very similar, the relative orientations of the CCHC and CCCC modules are slightly different in all three LIMs; in this respect, LIM1 domain of CRP1 bears more resemblance to CRIP than to LIM2. Interestingly, a recent report describing the solution structure of the N-terminal zinc-binding module of a LIM domain from the protein Lasp-1 demonstrated that the N-terminal module is capable of assuming a characteristic LIM fold independent of its C-terminal counterpart (*21*). Similarly, both the CCHC and CCCC metal-binding subdomains of a zyxin-derived LIM domain have been purified as soluble zinc metallopeptides (*35*). The two metal-binding modules of a LIM domain are separated by only two amino acids, and mutagenesis analysis has shown that these residues are important for the ability of a LIM domain from zyxin to bind to CRP (*35*); these residues may also contribute to the relative orientations of the two metal-binding cassettes. The evidence that even the LIM domains from CRP1, which display substantial sequence similarity, can exhibit differences in the orientation of their zinc-binding subdomains suggests a mechanism by which functional diversity may be conferred.

Previous biochemical and immunocytochemical studies of vertebrate CRPs have shown their ability to interact directly with elements of the actin cytoskeleton. Taken together with the results reported here, these findings suggest a model in which CRPs may serve to link two structural elements of the contractile machinery to enhance the mechanical resilience of the muscle (Figure 11). In particular, we would postulate that the N-terminal LIM-glycine module is critical for the ability of CRPs to interact with the actin-rich contractile machinery and that the C-terminal module is connected to some as yet undefined component of the muscle cytoarchitecture to stabilize the sarcomeric arrays during contraction.

ACKNOWLEDGMENT

We are grateful to Dr. M. Zawrotny and R. Edwards (UMBC, Howard Hughes Medical Institute) for technical support. M.C.B. is the recipient of a Faculty Research Award from the American Cancer Society. M.C.B. is also the recipient of a Faculty Research Award from the American Heart Association. C.H. was the recipient of an undergraduate research award from the Biology Department at the University of Utah, and P.P. was supported in part by a fellowship from the Philippe Foundation.

SUPPORTING INFORMATION AVAILABLE

Supporting Information containing the table of chemical shifts of CRP1 is available. This material is available free of charge via the Internet at http://pubs.acs.org.

REFERENCES

1. Louis, H. A., Pino, J. D., Schmeichel, K. L., Pomies, P., and Beckerle, M. C. (1997) *J. Biol. Chem. 272*, 27484−27491.
2. Crawford, A. W., Pino, J. D., and Beckerle, M. C. (1994) *J. Cell. Biol. 124*, 117−127.
3. Jain, M. K., FuJita, K. P., Hsieh, C. M., Endege, W. O., Sibinga, N. E., Yet, S. F., Kashiki, S., Lee, W. S., Perrella, M. A., Haber, E., and Lee, M. E. (1996) *J. Biol. Chem. 271*, 10194−10199.
4. Arber, S., Halder, G., and Caroni, P. (1994) *Cell 79*, 221−231.
5. Arber, S., Hunter, J. J., Ross, J., Jr., Hongo, M., Sansig, G., Borg, J., Perriard, J. C., Chien, K. R., and Caroni, P. (1997) *Cell 88*, 393−403.

6. Stronach, B. E., Siegrist, S. E., and Beckerle, M. C. (1996) *J. Cell Biol. 134*, 1179−1195.
7. Schmeichel, K. L., and Beckerle, M. C. (1994) *Cell 79*, 211−219.
8. Freyd, G., Kim, S. K., and Horvitz, R. (1990) *Nature 344*, 876−879.
9. Karlsson, O., Thor, S., Norberg, T., Ohlsson, H., and Edlund, T. (1990) *Nature 344*, 879−882.
10. Taira, M., Otani, H., Saint-Jeannet, J.-P., and Dawid, I. B. (1994) *Nature 372*, 677−679.
11. Barnes, J. D., Crosby, J. L., Jones, C. M., Wright, C. V. E., and Hogan, B. L. M. (1994) *Dev. Biol. 161*, 168−178.
12. Shawlot, W., and Behringer, R. R. (1995) *Nature 374*, 425−430.
13. Warren, A. J., Colledge, W. H., Carlton, M. B. L., Evans, M. J., Smith, A. J. H., and Rabbitts, T. H. (1994) *Cell 78*, 45−57.
14. Kosa, J. L., Michelsen, J. W., Louis, H. A., Olsen, J. I., Davis, D. R., Beckerle, M. C., and Winge, D. R. (1994) *Biochemistry 33*, 468−477.
15. Michelsen, J. W., Schmeichel, K. L., Beckerle, M. C., and Winge, D. R. (1993) *Proc. Natl. Acad. Sci. U.S.A. 90*, 4404−4408.
16. Michelsen, J. W., Sewell, A. K., Louis, H. A., Olsen, J. I., Davis, D. R., Winge, D. R., and Beckerle, M. C. (1994) *J. Biol. Chem. 269*, 11108−11113.
17. Archer, V. E., Breton, J., Sánchez-García, I., Osada, H., Forster, A., Thomson, A. J., and Rabbitts, T. H. (1994) *Proc. Natl. Acad. Sci. U.S.A. 91*, 316−320.
18. Sadler, I., Crawford, A. W., Michelsen, J. W., and Beckerle, M. C. (1992) *J. Cell. Biol. 119*, 1573−1587.
19. Pérez-Alvarado, G. C., Miles, C., Michelsen, J. W., Louis, H. A., Winge, D. R., Beckerle, M. C., and Summers, M. F. (1994) *Nat. Struct. Biol. 1*, 388−398.
20. Pérez-Alvarado, G. C., Kosa, J. L., Louis, H. A., Beckerle, M. C., Winge, D. R., and Summers, M. F. (1996) *J. Mol. Biol. 257*, 153−174.
21. Hammarström, A., Berndt, K. D., Sillard, R., Adermann, K., and Otting, G. (1996) *Biochemistry 35*, 12723−12732.
22. Konrat, R., Weiskirchen, R., Kräutler, B., and Bister, K. (1997) *J. Biol. Chem. 272*, 12001−12007.
23. Luisi, B. F., Xu, W. X., Otwinowshi, Z., Freedman, L. P., Yamamoto, K. R., and Sigler, P. B. (1991) *Nature 352*, 497−505.
24. Omichinski, J. G., Clore, G. M., Schaad, O., Felsenfeld, G., Trainor, C., Appella, E., Stahl, S. J., and Gronenborn, A. M. (1993) *Science 261*, 438−446.
25. Feuerstein, R., Wang, X., Song, D., Cooke, N. E., and Liebhaber, S. A. (1994) *Proc. Natl. Acad. Sci. U.S.A. 91*, 10655−10659.
26. Valge-Archer, V. E., Osada, H., Warren, A. J., Forster, A., Li, J., Baer, R., and Rabbitts, T. H. (1994) *Proc. Natl. Acad. Sci. U.S.A. 91*, 8617−8621.
27. Wadman, I., Li, J., Bash, R. O., Forster, A., Osada, H., Rabbitts, T. H., and Baer, R. (1994) *EMBO J. 13*, 4831−4839.
28. Wu, R.-Y., and Gill, G. N. (1994) *J. Biol. Chem. 269*, 25085−25090.
29. Bach, I., Rhodes, S. J., Pearse, R. V., Heinzel, T., Gloss, B., Scully, K. M., Sawchenko, P. E., and Rosenfeld, M. G. (1995) *Proc. Natl. Acad. Sci. U.S.A. 92*, 2720−2724.
30. Osada, H., Grutz, G., Axelson, H., Forster, A., and Rabbitts, T. H. (1995) *Proc. Natl. Ascad. Sci. U.S.A. 92*, 9585−9589.
31. Jurata, L. W., Kenny, D. A., and Gill, G. N. (1996) *Proc. Natl. Acad. Sci. U.S.A. 93*, 11693−111698.
32. Pomiès, P., Louis, H. A., and Beckerle, M. C. (1997) *J. Cell Biol. 139*, 157−168.
33. Fyrberg, E., Kelly, M., Ball, E., Fyrberg, C., and Reedy, M. C. (1990) *J. Cell. Biol. 110*, 1999−2011.
34. Crawford, A. W., and Beckerle, M. C. (1991) *J. Biol. Chem. 266*, 5847−5853.
35. Schmeichel, K. L., and Beckerle, M. C. (1997) *Mol. Biol. Cell 8*, 219−230.
36. Arber, S., and Caroni, P. (1996) *Genes Dev. 10*, 289−300.
37. Kong, Y., Flick, M. J., Kudla, A. J., and Konieczny, S. F. (1997) *Mol. Cell. Biol. 17*, 4750−4760.
38. Schmeichel, K. L., and Beckerle, M. C. (1998) *Biochem. J. 331* (3), 885−892.
39. Griesinger, C., Otting, G., Wüthrich, K., and Ernst, R. R. (1988) *J. Am. Chem. Soc. 110*, 7870−7872.
40. Brown, S. C., Weber, P. L., and Mueller, L. (1988) *J. Magn. Reson. 77*, 166−169.
41. Blake, P. R., Park, J. B., Bryant, F. O., Aono, S., Magnuson, J. K., Eccleston, E., Howard, J. B., Summers, M. F., and Adams, M. W. W. (1991) *Biochemistry 30*, 10885−10895.
42. Marion, D., and Bax, A. (1989) *J. Magn. Reson. 83*, 205−211.
43. Marion, D., Kay, L. E., Sparks, S. W., Torchia, D. A., and Bax, A. (1989) *J. Am. Chem. Soc. 111*, 1515−1517.
44. Pauly, J., LeRoux, P., Mishimura, B., and Macovski, A. (1991) *IEEE Trans. Med. Imaging*, 53.
45. Kay, L. E., Marion, D., and Bax, A. (1989) *J. Magn. Reson. 84*, 72−84.
46. Shinnar, M., Eleff, S., Subramanian, H., and Leigh, J. S. (1989) *Magn. Reson. Med. 12*, 74−80.
47. Bax, A., Ikura, M., Kay, L. E., and Zhu, G. (1991) *J. Magn. Reson. 91*, 174−178.
48. Zhu, G., Torchia, D. A., and Bax, A. (1993) *J. Magn. Reson., Ser. A 105*, 219−222.
49. Shaka, A. J., Keler, J., and Freeman, R. (1983) *J. Magn. Res. 53*, 313−340.
50. Johnson, B. A., and Blevins, R. A. (1994) *J. Biomol. NMR 4*, 603−614.
51. Güntert, P., Mumehnthaler, C., and Wüthrich, K. (1997) *J. Mol. Biol. 273*, 283−298.
52. Clore, G. M., Gronenborn, A. M., Nilges, M., and Ryan, C. A. (1987) *Biochemistry 26*, 8012−8023.
53. Weiskirchen, R., Pino, D. J., Macalma, T., Bister, K., and Beckerle, M. C. (1995) *J. Biol. Chem. 270*, 28946−28954.
54. Wüthrich, K. (1986) in *NMR of Proteins and Nucleic Acids*, John Wiley & Sons, New York.
55. Clore, G. M., and Gronenborn, A. M. (1991) *Science 252*, 1390−1399.
56. Blake, P. R., and Summers, M. F. (1994) in *Advances in Biophysical Chemistry*, pp 1−30, JAI Press Ltd., London, U.K.
57. Blake, P. B., Lee, B., Park, J.-B., Zhou, Z. H., Adams, M. W. W., and Summers, M. F. (1994) *New J. Chem. 18*, 387−395.
58. Spera, S., and Bax, A. (1991) *J. Am. Chem. Soc. 113*, 5490−5492.
59. Wishart, D. S., Sykes, B. D., and Richards, F. M. (1991) *J. Mol. Biol. 222*, 311−333.
60. Wishart, D. S., Sykes, B. D., and Richards, F. M. (1992) *Biochemistry 31*, 1647−1651.
61. Konrat, R., Weiskirchen, R., Bister, K., and Kräutler, B. (1998) *J. Am. Chem. Soc. 120*, 7127−7128.
62. Beckerle, M. C. (1997) *Bioessays 19*, 949−957.
63. Steinmetz, A. (1996) WWW web site, http://scilla.u-starsbg.fr/.
64. Kraulis, P. J. (1991) *J. Appl. Crystallogr. 24*, 946−950.
65. Bacon, D. J., and Anderson, W. F. (1988) *J. Mol. Graphics 6*, 219−220.

BI982036Y